ATMOSPHERIC SCIENCE

Bioaerosols are the dominant source of warm-temperature immersion-mode INPs and drive uncertainties in INP predictability

Gavin C. Cornwell[1,2]*, Christina S. McCluskey[3,4], Thomas C. J. Hill[3], Ezra T. Levin[3]†, Nicholas E. Rothfuss[5], Sheng-Lun Tai[1], Markus D. Petters[5]‡, Paul J. DeMott[3], Sonia Kreidenweis[3], Kimberly A. Prather[2,6], Susannah M. Burrows[1]

Ice-nucleating particles (INPs) are rare atmospheric aerosols that initiate primary ice formation, but accurately simulating their concentrations and variability in large-scale climate models remains a challenge. Doing so requires both simulating major particle sources and parameterizing their ice nucleation (IN) efficiency. Validating and improving model predictions of INP concentrations requires measuring their concentrations delineated by particle type. We present a method to speciate INP concentrations into contributions from dust, sea spray aerosol (SSA), and bioaerosol. Field campaign data from Bodega Bay, California, showed that bioaerosols were the primary source of INPs between −12° and −20°C, while dust was a minor source and SSA had little impact. We found that recent parameterizations for dust and SSA accurately predicted ambient INP concentrations. However, the model did not skillfully simulate bioaerosol INPs, suggesting a need for further research to identify major factors controlling their emissions and INP efficiency for improved representation in models.

INTRODUCTION

Ice-nucleating particles (INPs) are a subset of atmospheric aerosol that can initiate heterogeneous ice nucleation (IN). While they are rare [roughly 1 in 10^5 particles in ambient continental air is an active INP at −30°C (*1*)], these INPs can affect precipitation and the radiative properties of clouds due to their ability to induce glaciation, with important impacts on weather and climate (*2*–*6*). Immersion-mode INPs are of particular importance to freezing processes in mixed-phase clouds (*7*) and are the focus of this study. While many substances have been shown to nucleate ice, observational evidence suggests that only a small number of particle types must be represented to adequately predict INPs in climate models, including mineral and soil dusts, sea spray, and biological INPs (hereafter "bio-INPs") (*8*, *9*).

While dust particles are well understood to be the globally most abundant source of immersion-mode INPs in boundary-layer air at colder temperatures [e.g., below −25°C; (*10*, *11*)], previous studies suggest that bio-INPs are likely the primary source of INPs at temperatures above −15°C (*12*). Global simulations incorporating bio-INPs have found that they may contribute to droplet freezing in warm portions of mid-latitude clouds (*13*).

The contribution of bio-INPs to freezing at warmer temperatures is important due to the potential impacts on subsequent cloud development. After the initial formation of primary cloud ice, cloud glaciation can be further accelerated by secondary ice production (SIP) mechanisms (*14*) that lead to the formation of additional cloud ice. High-resolution modeling studies suggest that certain clouds are particularly sensitive to warm-temperature INPs when SIP is accounted for, with impacts on both surface precipitation and cloud radiative properties (*4*, *15*). More broadly, advances in remote sensing have recently made it possible to identify SIP in clouds, and have shown that SIP is particularly important at temperatures ranging from −5° to −20°C (*16*). Consequently, bio-INPs, which are active at warmer freezing temperatures, may be particularly impactful for climate.

Despite their importance, bio-INPs have proven challenging to measure and identify in the atmosphere, and models of bio-INP impacts on clouds and climate consequently have lacked adequate validation datasets. Most previous studies of bio-INPs in the ambient atmosphere have relied on indirect methods to identify bio-INPs, such as heat and peroxide treatments (*17*) that deactivate biological and organic INPs. These methods are inexpensive and readily accessible, but the potential for deactivation of other INP types by these treatments introduces inherent uncertainties in their interpretation (*18*). Other studies have used correlation analysis to show associations between elevated biological particle and INP concentrations (*19*), but have not quantified the contributions of bio-INPs to the total INP population.

In this work, we use a unique measurement dataset to conclusively attribute warm-temperature INPs to bioaerosol. At colder temperatures (ca. −30°C), we directly observe dust and sea spray INPs and show that both can be predicted well by current INP parameterizations. After accounting for dust and sea spray INPs, the remaining variability in observed INPs at warmer freezing temperatures (−12° to −20°C) is correlated with a class of fluorescent

[1]Atmospheric Science and Global Change Division, Pacific Northwest National Laboratory, Richland, WA 99352, USA. [2]Department of Chemistry and Biochemistry, University of California, San Diego, La Jolla, CA 92093, USA. [3]Department of Atmospheric Science, Colorado State University, Fort Collins, CO 80523, USA. [4]National Center for Atmospheric Research, Boulder, CO 80305, USA. [5]Department of Marine, Earth, and Atmospheric Sciences, North Carolina State University, Raleigh, NC 27605, USA. [6]Scripps Institution of Oceanography, University of California, San Diego, La Jolla, CA 92037, USA.
*Corresponding author. Email: gavin.cornwell@pnnl.gov
†Present address: Colorado Department of Public Health and Environment (CDPHE), Glendale, CO 80246, USA.
‡Present address: Department of Chemical and Environmental Engineering, Bourns College of Engineering, Center for Environmental Research and Technology (CE-CERT), University of California, Riverside, Riverside, CA 92507, USA.

bioaerosol, FP3, which is operationally defined by their measurement from a fluorescence-sensitive optical particle counter. By developing a linear relationship between FP3 particles and bio-INPs, we show that bio-INPs comprised more than 60% of INPs in this temperature range. Using this unique dataset, we evaluate the ability of present-day models to adequately simulate ambient immersion-mode INPs from multiple particle types at both warmer and colder freezing temperatures. We show that the leading obstacle to accurate simulation of total INP concentrations by an atmospheric model during a field campaign in California is the inaccurate representation of bio-INPs.

RESULTS

All measurements used in this study were collected at the Bodega Marine Laboratory in Bodega Bay, CA (38.3186°N, 123.0716°W) during the CalWater-2015 field campaign. Our previous work showed that approximately 90% of INPs at Bodega Bay could be classified as either dust, sea spray aerosol (SSA), or bioaerosol (*20*). We considered other particle types that have been shown to nucleate ice, namely, soot and organic aerosol. However, these particle types generally have low IN activity in the mixed-phase cloud regime (*21*) and would not be expected to contribute substantially to INP populations in this study given the locations (*22*, *23*), and thus, we neglect any potential contributions. The focus of this study is testing our predictive understanding of the variability in ambient concentrations of each of these INP types, with the goal of understanding whether adequate simulation of each INP type is currently achievable in atmospheric models.

We posit that for simulation of INPs in models to be considered adequate, prediction errors must be less than an order of magnitude for most observations. High-resolution cloud modeling shows that clouds can be sensitive to INP perturbations of more than one order of magnitude (*5*), suggesting that this is a necessary criterion for simulation of cloud processes. Global aerosol models are often able to predict aerosol loadings within an order of magnitude [e.g., (*24*)], suggesting that this criterion may be achievable by large-scale models.

We therefore use two primary metrics to evaluate our ability to correctly predict total INP concentrations: (i) the fraction of total speciated INPs within a factor of 2 of the total predicted INPs (F_2), and (ii) the fraction of total speciated INPs within a factor of 10 of the total predicted INPs (F_{10}). We consider prediction of INPs to be successful on these metrics if we are able to achieve $F_2 \geq 0.5$ and $F_{10} \geq 0.8$. In addition, the mean bias in predicted INPs should be less than an order of magnitude, as measured by a modified normalized mean bias (MNMB) less than 1. Last, a high correlation between observed and predicted INPs, as measured by the Pearson correlation coefficient (r), is desirable.

In this context, we discuss here four separate analyses that test predictive understanding: (i) a closure analysis for directly detected dust and SSA INPs at colder temperatures; (ii) an apportionment of INPs at warmer freezing temperatures to dust, sea spray, and bio-INPs; (iii) an analysis of model predictive skill for cold-temperature INPs; and (iv) an analysis of model predictive skill for warm-temperature INPs (Fig. 1). Although the observations we use for this study are taken from a single field campaign, they provide a direct and quantitative corroboration for a growing body of studies suggesting that bio-INPs play a critical role at warmer freezing temperatures in many locations globally (*9*, *12*, *25*).

Closure analysis for INPs directly detected at freezing temperatures ca. −30°C

We first perform a closure analysis, testing the ability of current INP parameterizations to adequately predict both dust and sea spray INP concentrations ($N_{INP,x}$) for each particle type x at colder freezing temperatures from −28° to −33°C. INPs were quantified using the Colorado State University (CSU) Continuous Flow Diffusion Chamber (CFDC). In addition, INPs were aerodynamically separated and chemically classified by an aerosol time-of-flight mass spectrometer (ATOFMS) (*26*) in a residual characterization experiment (*20*).

We compare observed INP concentrations with those predicted using active site density (n_s)–based parameterizations following the equation

$$N_{INP,x} = n_{s,x} A_x$$

where $n_{s,x}$ [m^{-2}] is the active site density for particle type x (dust, sea spray, or bio-INP) and A_x is the total surface area concentration of particle type x (m^2 $liter^{-1}$). We parameterize dust and SSA INPs following (*27*, *28*), respectively. The parameterization for SSA has an uncertainty range of a factor of 2, while the dust parameterization has no uncertainty range. Type-specific surface areas A_{Dust} and A_{SSA} were derived by combining single-particle classifications with the size distribution measured by an aerodynamic particle sizer (APS) (APS 3321, TSI Inc.), as in previous studies (*29*, *30*).

Figure 2 (A and B) shows the speciated INPs for SSA and dust from the residual characterization measurement versus those predicted using existing parameterizations and ambient aerosol measurements. Excellent agreement was found between the speciated and predicted INPs for both SSA and dust, with a Pearson correlation coefficient of $r = 0.9$ and $r = 0.8$, and an average overprediction of only 33 and 41% (MNMB of 0.33 and 0.41), respectively. This closure analysis demonstrates that $N_{INP,x}$ can be successfully predicted at colder temperatures using recent INP parameterizations, when the available surface area for each particle type is known.

We also note that while SSA is an important source of INPs over remote ocean regions where continental aerosols are scarce (*3*, *31*), SSA did not notably contribute to INPs in this study. Despite the proximity to the ocean, we observed only about five times more particle surface area for SSA than for dust (fig. S1). Dust particles typically have IN activities two to three orders of magnitude greater than SSA particles at the same temperature (*27*, *28*, *30*), which explains why dust INPs were much more prevalent than SSA INPs at this coastal site. This is consistent with modeling studies suggesting that SSA particles are an important source of INPs only at locations distant from land (*31*).

INP apportionment and closure at freezing temperatures between −12° and −20°C

Total immersion-mode INPs at warmer freezing temperatures between −12° and −20°C were quantified by the North Carolina State University (NCSU) Cold Stage (*32*). We use single-particle measurements from a wideband integrated bioaerosol sensor (WIBS) (WIBS-4, DMT Inc.) to support our attribution of bio-INPs in this temperature range. At these warmer temperatures,

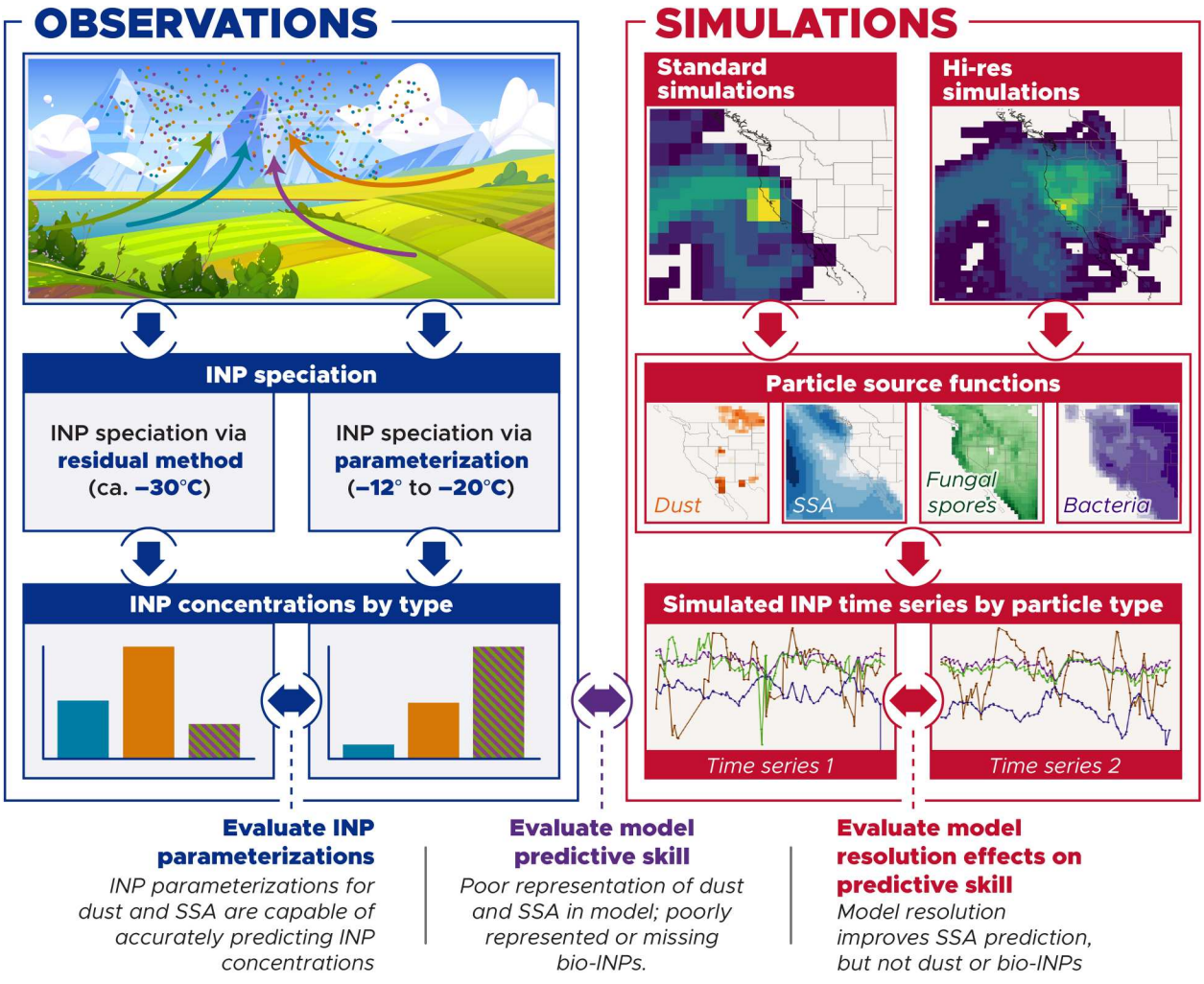

Fig. 1. Overview of the methodology used in this study. We take two different approaches to speciate INP concentrations using single-particle techniques. The first approach uses the direct measurements of ice crystal residuals with an SPMS to fractionate INP concentrations. The second approach uses single-particle measurements in tandem with size distributions to derive speciated particle surface area distributions. We then apply particle type–specific active site density n_s parameterizations to calculate INP concentrations for different particle types. These two approaches can be used to evaluate the representativeness of dust and SSA INP parameterizations. We take a Lagrangian approach to evaluate model predictive skill. We use a turbulent dispersion model, FLEXPART, to calculate source-receptor influence footprints and combine these source-receptor footprints with particle source functions for dust, SSA, fungal spores, and bacteria along with appropriate n_s parameterizations to predict INP concentrations. The predictive skill of the model is evaluated using the speciated INP measurements. In addition, using high- and low-resolution meteorological data to drive the Lagrangian simulations allows us to assess how model resolution affects our prediction of INP concentrations.

INP concentrations correlate strongly with the FP3 particle class, a subset of fluorescent particles measured by the WIBS-4, characterized by their very high fluorescent signal in the tryptophan channel (Fig. 3) (*33*). Similar associations have been observed in previous field experiments (*34*, *35*), suggesting a strong contribution of bioaerosols to warm-temperature INPs. Therefore, we posit that the FP3 particle type is a reliable proxy for the concentration of bio-INPs during this field study.

Because too few INPs are active at these warmer temperatures to allow a residual characterization experiment, we take a different approach to speciate INPs in this temperature range. We first extend our calculation of dust and SSA INPs using n_s-based parameterizations to the warmer temperature range. For bioaerosol, the uncertainties in both the measured size distribution and available INP parameterizations are large enough to prohibit this approach. Instead, we parameterize bio-INP number concentration by applying a linear, temperature-dependent scaling factor to the FP3 concentration (fig. S2). This scaling factor was derived from a sum-of-least squares best fit to the residual concentration of INPs after first subtracting the concentrations of dust and SSA INPs (see Materials and Methods for more details). While the ATOFMS and WIBS have different measurement ranges and detection methods, and thus would not be expected to measure the same particles, previous work has found a moderate correlation (r = 0.73) between bioparticles measured by the ATOFMS and the FP3 particle class (*33*).

Notably, bioaerosols were the dominant source of INPs at all temperatures between −12° and −20°C (binned in one-degree intervals; Fig. 4), comprising more than 60% of the INPs active in this temperature range. Dust particles were a minor INP source at −12°C, but increased in importance at colder temperatures,

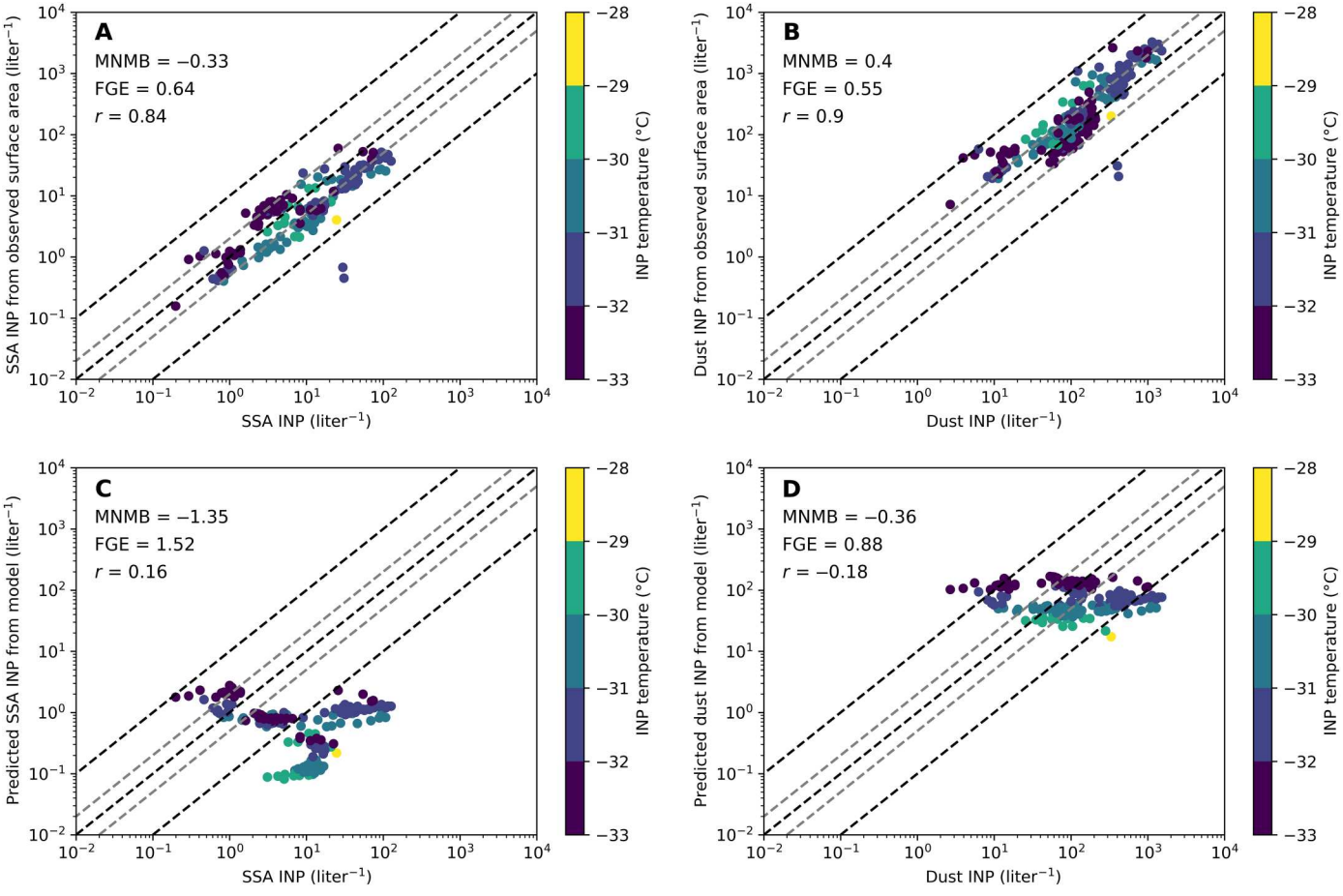

Fig. 2. Scatter plots of predictions of speciated INPs, on the basis of parameterizations and aerosol measurements, versus speciated INPs based on residual experiments. Marker color shows the temperature at which the measurement was collected. The top panels show relatively good agreement between speciated INPs predicted from aerosol size distributions for SSA (**A**) and dust (**B**). The bottom panels show the speciated INPs versus those predicted from simulations for SSA (**C**) and dust (**D**). MNMB, fractional gross error (FGE), and *r* are shown for each plot.

contributing 10 to 40% of the INPs active at −19°C. These results are consistent with previous literature showing that bio-INPs make up a greater fraction of continental boundary layer INPs at warmer temperatures than at colder temperatures (*19*, *25*, *36*).

Next, we evaluate aerosol-INP closure for warm-temperature INPs, by comparing the total of our dust, sea spray, and bio-INP proxies with the total INPs quantified via droplet freezing. Closure exceeded our requirements, with agreement within a factor of 2 achieved 40 to 50% of the time. Agreement within a factor of 10 was achieved 80 to 90% of the time for temperatures warmer than −18°C (fig. S3). MNMB is less than 1 for temperatures warmer than −17°C (Fig. 4). The correlation between predicted and measured INP concentrations ranged from 0.66 to 0.86 across all temperatures (Fig. 4D). Overall, we conclude that aerosol-INP closure was achieved to within the precision required for atmospheric models at temperatures between −12° and −17°C, while errors from −17° to −20°C were slightly greater than our established criteria.

An unavoidable limitation of our approach to warm-temperature closure is that the prediction of bio-INPs relies in part on the total INP measurement, which is also used to evaluate closure. Therefore, we also examined independent sources of evidence to corroborate our attribution of bio-INPs. First, we performed heat treatment experiments on an independent INP dataset using filters processed in the CSU ice spectrometer (IS) for select periods when our method predicts high bio-INPs and low bio-INPs. These experiments showed that more INPs were deactivated during periods of high bio-INPs, which qualitatively corroborates our attribution method for bio-INPs (fig. S4).

Second, we note an increase in bio-INPs following each of two observed atmospheric river events (fig. S5). A similar phenomenon has been observed in previous field experiments where bioaerosol, total INP, and heat-sensitive INP concentrations all increased in tandem during and after rainfall (*37*–*39*). The consistency of this study with previous studies demonstrating a connection between rain events and bio-INPs adds further corroborating support to our conclusions.

Predictive skill for INP concentrations at freezing temperatures ca. −30°C

Having established that aerosol-INP closure is achieved using current INP parameterizations for SSA and dust, we next applied these parameterizations to model-simulated aerosol and quantified model predictive skill. By separately quantifying closure errors and

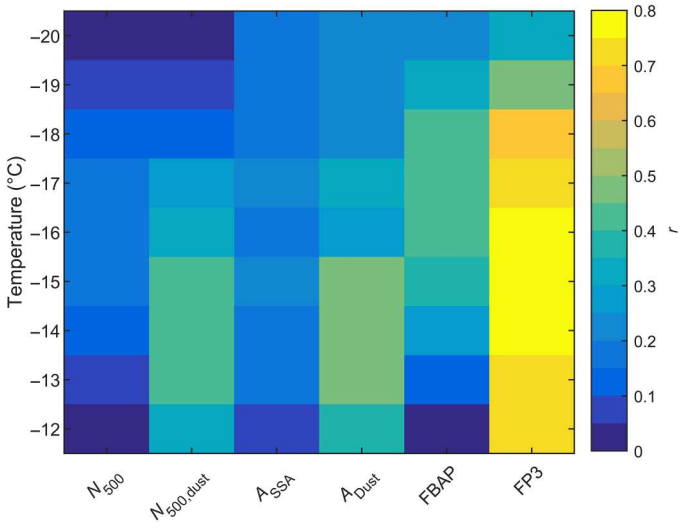

Fig. 3. Heatmap showing the Pearson correlation coefficients (*r*) between INP concentrations and aerosol observations. N_{500} is the total number concentration of particles larger than 0.5 μm, $N_{500,dust}$ is the number concentration of dust particles larger than 0.5 μm, A_{SSA} and A_{Dust} are the total particle surface area concentrations for SSA and dust, respectively, while FBAP (total fluorescent biological aerosol particles) and FP3 are the particle class concentrations measured by the WIBS.

model predictive skill, we can examine the relative contributions of errors in INP parameterizations to our ability to successfully simulate INP concentrations at this site.

We used a Lagrangian model, FLEXPART (*40*), to simulate INP transport and concentrations at the Bodega Bay site. Lagrangian methods are well suited when observations are made at a single point and sources are regionally widespread, as is the case in this study. To simulate INPs from dust and sea spray, we combined Lagrangian source-receptor footprints (*41*) with surface emission functions for each particle type. The Lagrangian model was driven by 0.5° input data (hereafter the standard simulations), and the emission functions of sea spray and dust were taken from a global climate model simulation. Figure 2 (C and D) shows the modeled concentrations for SSA and dust versus those measured via the residual experiments. Neither particle type is predicted well; SSA is underpredicted severely (MNMB = −1.35), while the simulation of dust shows less bias (MNMB = −0.36). The correlation between simulated and observed INPs is poor for both SSA (r = 0.17) and dust (r = 0.18). Given the good closure demonstrated in Fig. 2 (A and B), we conclude that our inability to accurately represent SSA and dust INP concentrations is caused by deficiencies in the model's simulation of SSA and dust particles.

Predictive skill for INP concentrations at freezing temperatures between −12° and −20°C

To extend our analysis of model predictive skill to warmer temperatures, we added representations of bacterial and fungal spore INPs. Bacterial emissions were prescribed as a fixed emission map (*42*), and fungal spore emissions were parameterized on the basis of satellite and meteorological variables from reanalysis data (*43*). Simulated INP concentrations were calculated using n_s parameterizations for dust (*27*) and SSA (*28*). For bacterial and fungal spores, most published INP parameterizations are based on measurements of individual microbial species isolated in a laboratory environment. However, in light of the well-documented discrepancies in INP activity spanning several orders of magnitude between various bioaerosol types (*10*, *12*, *44*), it appears imprudent to assume that any individual species is representative for ambient bio-INPs. Therefore, we use recently proposed bacterial and fungal spore INP parameterizations that were derived from measurements of ambient bioaerosol (*45*). We compared the sum of simulated bacterial and fungal spore INP concentrations with observed bio-INPs.

Figure 5 shows the ratio of simulated to observed INPs for the speciated and total INP concentrations. Across all temperatures, we predict both dust and SSA INPs adequately, despite moderately underpredicting dust INPs (median predict-to-observed ratio of 0.2 to 0.4) and moderately overpredicting SSA INPs (median ratio of 3.6 to 4.6). However, we substantially underpredict bio-INPs, particularly at warmer temperatures, with a median ratio of 0.10 at −12°C. Because most of the INPs are bioaerosol at warmer temperatures, this causes a notable underprediction of total INPs (Fig. 5D). These results show that without improved representations of the sources and IN activities of bio-INPs, models will struggle to simulate total INP concentrations at warmer temperatures.

DISCUSSION

Clarifying the leading sources of error in INP predictive skill at Bodega Bay

Ultimately, we are interested in identifying the structural causes of poor predictive skill for bio-INPs. We expect these to be driven primarily by three potential categories of errors: (i) uncertainties in the parameterizations for the IN activity of each particle type, (ii) inadequate source functions for the surface emissions of relevant particle types, and (iii) inadequate simulation of aerosol transport. In this section, we examine each of these potential categories of error in turn.

First, we consider errors associated with INP parameterizations. Laboratory studies of the impact of atmospheric aging have found that they can affect IN activity, albeit with inconsistent outcomes. For instance, aging with sulfuric acid can either greatly reduce the immersion mode IN activity (*46*) or have little effect. The IN activity of biomass burning can actually increase due to photochemical oxidation (*47*), whereas surrogate secondary aging has little to no impact on the IN activity of dust (*21*). Given these conflicting findings and the dearth of knowledge surrounding how to parameterize the IN activity of aged particles generally, we have made the decision not to account for potential aging effects on IN activity within the scope of our study. However, as shown in Fig. 2, the INP parameterizations for dust and SSA perform well at freezing temperatures ca. −30°C when aerosol properties are known. While we do not have direct measurements of INPs at warmer temperatures, it is reasonable to expect similar results at other temperatures within the valid range of the parameterizations. We therefore conclude that uncertainties in sea spray and dust INP parameterizations, or potential effects of atmospheric aging on IN activity, are likely only a minor source of error in this study.

At warmer freezing temperatures, however, poor predictive skill for bio-INPs suggests that these parameterizations may be a source of error. One potential explanation is that bio-INPs may exhibit variations in their INP efficiency that are not adequately captured by

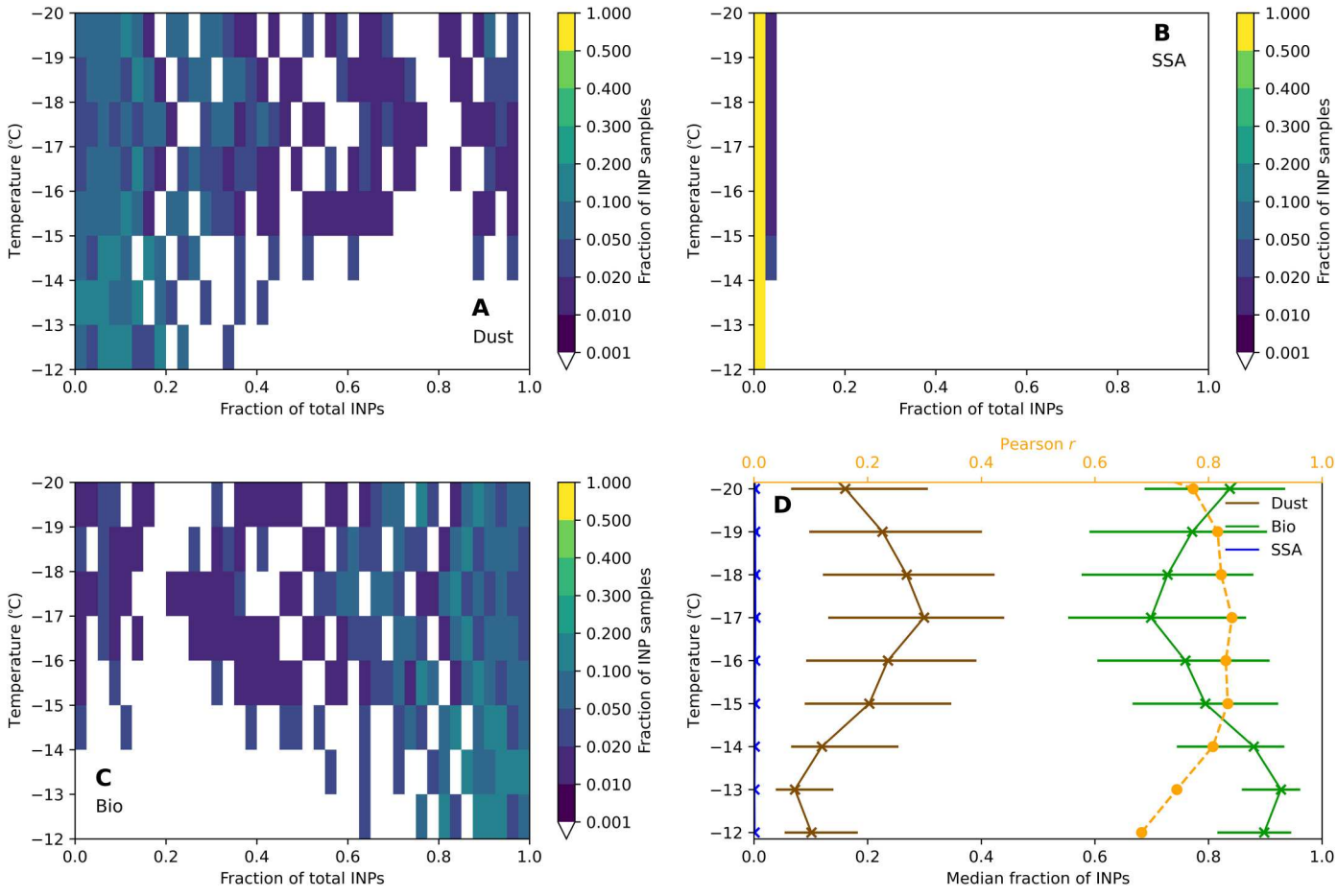

Fig. 4. Heatmaps of the fraction of speciated INPs as a function of temperature. Panels show the fraction for (**A**) dust, (**B**) SSA, and (**C**) bio-INPs (Bio). Figure shading shows the fraction of INP samples between the upper and lower bounds of that bin, where brighter (darker) colors indicate bins with higher (lower) frequency of occurrence of that species's fractional contribution (*x* axis) at a given temperature (*y* axis). (**D**) Median estimated fraction of INPs from dust (brown), SSA (blue), and bio-INPs (green). The horizontal bars show the interquartile ranges. The Pearson correlation coefficient *r* for the fit between the total speciated INPs and measured INPs is also shown.

current parameterizations. Development of robust bio-INP parameterizations has proven challenging due to the small sampling statistics achieved at warmer temperatures where bio-INPs are important, and the inherent complexity of bioaerosols. Laboratory studies have found that the IN activity of bacterial and fungal spores can vary substantially across different species (*12*, *48*, *49*). Because the species composition of airborne fungal and bacterial communities exhibits considerable geographic variability (*50*, *51*), it is reasonable to expect that the IN activity of airborne fungal spores or bacteria may differ between geographic regions. The bio-INP parameterizations we have used were developed on the basis of a small number of samples from the Amazon rain forest (*45*) and may not be representative for the bio-INPs we observed in coastal California.

Another potential source of error is the occurrence of changes in the efficiency of bio-INPs as a function of environmental conditions. For example, bio-INP efficiency can be altered by atmospheric processes such as photo-oxidation (*52*), and some bacteria actively modify their surface chemistry in response to environmental conditions (*53*). The effects of environmental conditions are presently not sufficiently well understood to be accounted for in bio-INP parameterizations. Our findings suggest a need for further research to develop, validate, and improve parameterizations of INPs and their environmental transformations. While experimental challenges remain, recent advances in INP measurement technologies show promise to markedly improve the observational basis for such studies in the near future, e.g., by increasing throughput and facilitating single-particle microspectroscopic analysis of INPs (*54*).

Next, we consider errors caused by inadequate—or missing—source functions. While we have documented that simulation errors cause model-observation mismatches for dust and SSA INPs (Fig. 2), the largest errors in this study are associated with our simulation of bio-INPs (Fig. 5). The simulation of bioaerosol emissions is acknowledged to be fraught with uncertainties, and only a small number of previous studies have evaluated simulations of fungal spores and bacteria using independently collected datasets. These studies showed examples of both good agreement and poor agreement with locally measured vertical profiles (*43*, *55*) and large-scale geographic variations (*43*, *56*). This suggests that while models can simulate bioaerosol concentrations that are broadly consistent with order-of-magnitude concentrations

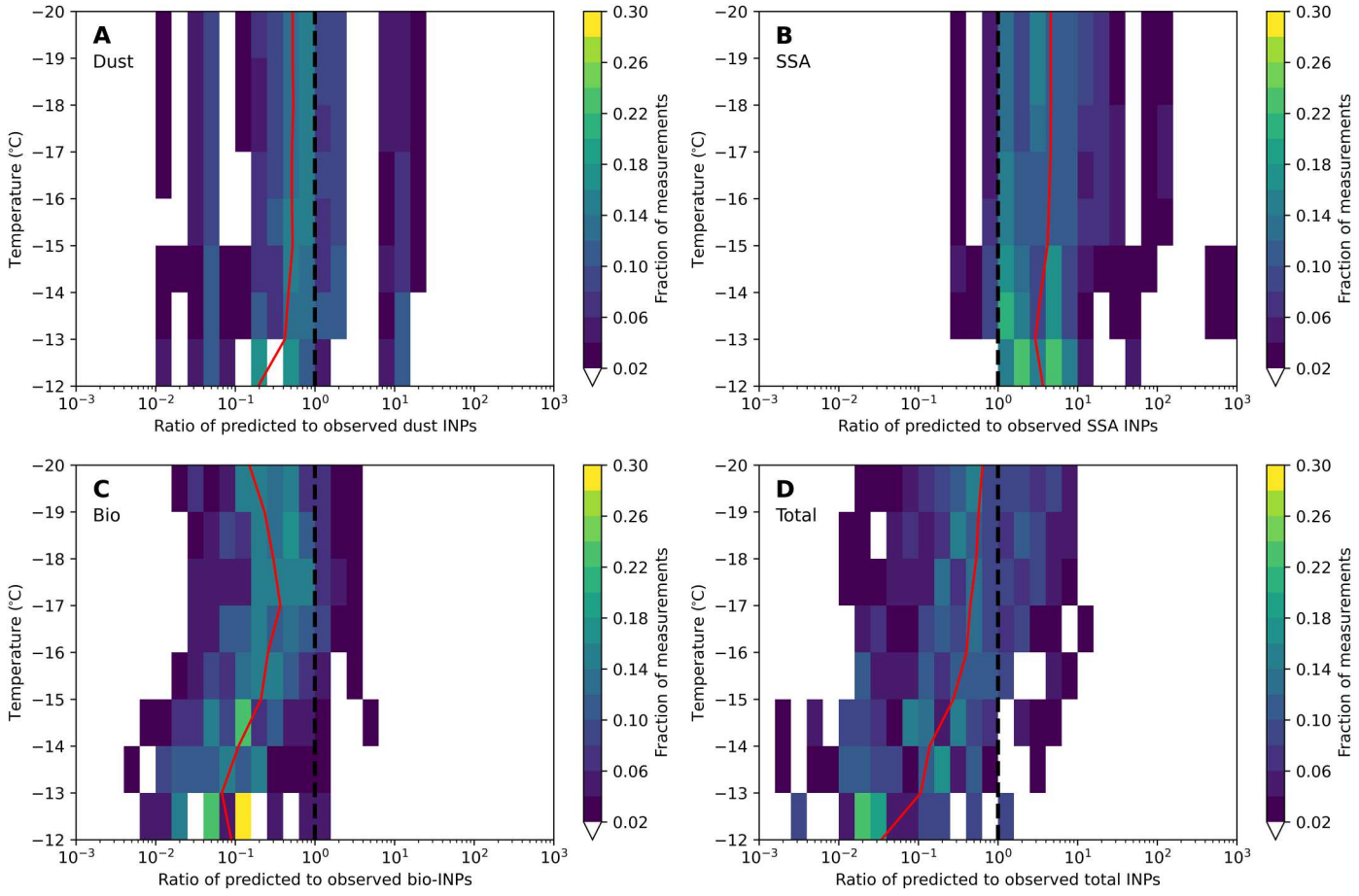

Fig. 5. Heatmaps of the ratios of predicted to observed INPs as a function of temperature. Panels show the rations for (**A**) dust, (**B**) SSA, (**C**) bio-INPs, and (**D**) total INPs. Red lines show the median values for each temperature. Dashed black lines show the 1:1 line where predicted INPs agree with observed INPs.

observed in the atmosphere (fig. S6), environmental factors driving variability in bioaerosol emissions and concentrations are likely not fully captured by current models. For example, models currently do not represent the previously noted increases in bio-INP concentrations that frequently follow rainfall (*25*, *33*, *34*, *36*, *37*). Likewise, our simulations did not predict the increase in bio-INPs following precipitation (fig. S5). More work is needed to improve source functions for bio-INPs and more fully incorporate the observed dependence of bio-INP sources on both surface properties and environmental conditions.

One challenge in developing such source functions is that the identity and nature of the bioaerosols that contribute to bio-INPs is still not fully understood. There is ample evidence supporting a link between INPs and either total fluorescent particles (*37*) or the FP3 subset of fluorescent particles (*33*, *34*). However, the exact identity of these fluorescing particles has not yet been clarified, and it remains challenging to identify better proxies for bio-INP that can be readily measured in the environment. For example, bio-INPs correlate poorly with the relative abundances of ice-nucleating bacteria identified via sequencing analyses (*57*, *58*) but appear to be somewhat related to total bacterial abundance (*58*).

Additional bio-INP sources may exist that are beyond the scope of the current study. While we have focused here on fungal spores and bacteria, several other particle types have been identified as potential sources of bio-INPs, such as subpollen particles (*59*), fungal spore fragments (*60*), cellulose-containing particles (*61*), and intermittently or seasonally present oceanic bio-INPs (*62*). Because of experimental challenges, the quantitative relevance of these particles in the atmosphere is still poorly understood, we did not include them here, but we also cannot exclude them as potentially important sources of bio-INPs. Overall, the totality of the evidence suggests a lack of a fundamental understanding of bioaerosol types and the mechanisms by which they are emitted from the biosphere into the atmosphere. Fundamental process studies are needed to establish confidence in model extrapolation of bio-INP based on these empirical parameterizations in response to a changing biosphere.

We now turn to our third potential category of errors, those associated with simulated aerosol transport. In particular, the effect of localized circulation patterns such as land-sea breezes and flow near local topographic features like the Sierra Nevada could be missed in coarse-resolution meteorological simulations. We therefore investigated whether higher-resolution meteorological data could improve the model's predictive skill. We performed a second set of Lagrangian simulations using higher-resolution meteorological input data (4-km resolution, simulated using an observationally constrained version of the Weather Research and Forecasting Model, see Supplementary Materials for more details). Using these higher-resolution

input data improved our prediction of SSA INPs, but not dust and bio-INPs (fig. S7). The improved prediction of SSA INPs is likely attributable to an improved ability to represent small-scale transport patterns around the coastline. The lack of improvement for dust, by contrast, indicates that errors in dust prediction were not primarily caused by model resolution. Dust prediction errors may be driven by sources for which we lack adequate emission representations, including potential anthropogenic sources near the site (e.g., traffic and construction) and in the surrounding region (e.g., agriculture). Our predictions of bio-INPs were equally poor regardless of the resolution of the meteorological fields. While we cannot exclude model representations of physical loss transformation and processes as a potential cause of simulation bias, we can conclude that model resolution was not a leading source of INP prediction errors during this campaign.

Atmospheric implications

We have shown that bio-INPs are an important source of warm-temperature immersion freezing INPs at this measurement site. Using a combination of aerosol size, composition, IN parameterizations, and IN measurements, we speciated the relative contributions of dust, SSA, and bioaerosol to INP populations.

We used a Lagrangian modeling approach to simulate INP concentrations at the site, and find good agreement with dust and SSA, but poor agreement with bio-INPs. Our conclusion that bioaerosols are a crucial source of warm-temperature INPs implies that failing to accurately simulate their prevalence results in poor simulation of total INP concentrations at temperatures warmer than −15°C. While our focus here is on a detailed analysis of a single field campaign, a growing number of recent studies implicate bio-INPs as a critical source of warm-temperature INPs at a variety of locations, which suggests that this conclusion is broadly generalizable to many locations and times globally (*12*, *19*, *25*, *63*, *64*). We conclude that an improved fundamental understanding of the sources of bio-INPs and the environmental factors controlling their variability is required to improve and build confidence in parameterizations of bio-INP emissions and efficiency, and their dependencies on environmental factors.

In light of the complex nature of bio-INPs, it will likely prove prohibitively difficult to establish an inventory of individual bio-INP species and their responses to environmental conditions that contains sufficient information to be usefully extrapolated to observed atmospheric bioaerosol populations or confidently applied in atmospheric models. Instead, future studies, enabled by novel measurement technologies, should focus on field measurements that identify and attribute ambient bioaerosol and INPs in different ecosystems and environmental conditions. This approach will enable the scientific community to build an improved understanding of which ecosystem or environmental variables have substantial impacts on bio-INPs in the ambient atmosphere, and which variables can be confidently neglected when developing predictive models for bio-INPs. Laboratory experiments can provide complementary perspectives, for example, by isolating chemical or physical transformation mechanisms that may modify the INP availability and effectiveness of bioaerosols in the atmosphere. Last, improved understanding is required regarding the sensitivity of different cloud regimes to warm-temperature INPs, to clarify when and where adequate simulation of bio-INPs matters for clouds and climate. Addressing these research priorities to develop a more comprehensive understanding of the atmospheric variability of bio-INPs—and their impacts in different cloud regimes—will require joint efforts of the cloud modeling, aerosol modeling, aerosol measurement, and INP measurement communities.

MATERIALS AND METHODS

Field measurement site

Field measurements of aerosol size, number, composition, and microphysical properties were collected at Bodega Marine Laboratory in Bodega Bay, CA (38.3186°N, 123.0716°W) as part of the CalWater-2015 field campaign. Measurements were collected from 14 January to 8 March 2015. These measurements have been described before (*65*), so we provide only a short overview. Two mobile sampling laboratories were deployed to the site with instruments for the measurement of aerosol number, size, composition, and microphysical properties. Bioaerosol concentrations, black carbon mass, and gas-phase tracer concentrations were also measured, while filter and impinger samples were collected for offline analysis. A meteorology station owned and operated by the National Oceanic and Atmospheric Administration′s Earth System Research Laboratory was located ~100 m north of the site.

INP measurements

NCSU Cold Stage

Ambient aerosol was sampled for offline INP measurements using a three-piece 20-ml impinger sampler (SKC Inc., BioSampler). Impingers were located ~10 m away from two sampling trailers, at a height of approximately 0.3 m. The impinger sampled ambient air at a flow rate of 12.5 liters min^{-1} for a duration of approximately 4 hours. The INP concentrations of these ambient samples were measured using the NCSU Cold Stage (*33*). Because of the difference in height between the impingers and the rest of the measurements (roughly 3 to 4 m), we have scaled these measurements down by a factor of 5 to align with measurements from the CSU IS (see Supplementary Text for more information).

CSU ice spectrometer

Filters were at Bodega Bay for subsequent INP analysis with the CSU IS, which can investigate immersion freezing across a temperature range of 0 to about −27°C (*17*). Precleaned filters were preloaded into sterile, open-faced Nalgene filter units (Thermo Fisher Scientific Inc.) and placed beneath a rain shield on top of the sampling trailer. Before the study, all sample collection filters were cleaned in a laminar flow cabinet by soaking in 10% H_2O_2 for 10 min followed by three rinses in deionized water, the last of which had been filtered through a 0.02-μm-pore-diameter filter (Anotop 25-mm syringe filter, Whatman) and drying on foil.

After sampling, filters were transferred from filter holders and Nalgene units using cleaned plastic forceps and stored at −20°C in 60-mm-diameter petri dishes (CELLTREAT). For resuspension of particles, filters were placed in sterile 50-ml Falcon polypropylene tubes (Corning Life Sciences), 5 to 6 ml of 0.02-μm-pore-diameter filtered deionized water were added, and particles were resuspended by tumbling on Roto-Torque (Cole-Palmer) at 60 cycles/min for 20 min. Within a laminar flow cabinet, 32 × 50-μl aliquots of each suspension were transferred into sterile, 96-well polymerase chain reaction trays (Life Science Products Inc.), and the plates were transferred to the IS blocks. Immersion freezing temperature spectra were obtained from the IS following previously documented

procedures (*61*). Frozen wells were monitored as temperature was lowered at 0.33°C min^{-1} under aspiration of the instrument headspace with 0.5 to 1 liter min^{-1} of cooled, filtered (HEPA-CAP, Whatman) nitrogen. Frozen wells were counted at 0.5° or 1°C intervals to a limit of −27°C, and cumulative numbers of INPs (ml^{-1}) of suspension were estimated using

$$N_{INP} = \frac{-\ln(f)}{V_i}$$

where f is the proportion of droplets not frozen and V_i is the volume of each aliquot (*66*). Filter blanks (loaded into in-line filter units and loaded into and removed from the sampling platform) were processed to obtain background INP spectra. At each temperature, INPs in the blank were subtracted from sample measures in suspension, and then measured INPs in the total volume of suspension were converted to ambient INP concentrations ($liter^{-1}$) using the liters of air sampled. Binomial sampling confidence intervals (95%) were derived using previously established methods (*67*).

An additional subset of samples was selected for heat treatment to quantify the contributions of heat-labile INPs, assumed to be proteinaceous. Samples were heated to 95°C for 20 min, and the sample was reanalyzed to determine the reduction in INP concentrations (*17*). The difference between total INPs and the INPs remaining after the heat treatment were determined to be bio-INPs.

Bioaerosol concentrations

The WIBS (WIBS-4A, Droplet Measurement Technologies Inc.) measures the size, asymmetry factor, and fluorescence signal for individual particles from 0.5 to 20 μm. Fluorescence is measured in three different channels: FL1, excitation of 280 nm, emission of 310 to 400 nm; FL2, excitation of 280 nm, emission of 420 to 650 nm; and FL3, excitation of 370 nm, emission of 420 to 650 nm. The detection of fluorescent particles from 0.5 to 0.8 μm is limited by the sensitivity of the instrument's detectors (*68*); therefore, we limit fluorescent particles to the size range of 0.8 to 20 μm. Background fluorescence signal was calculated following (*69*) where we force-triggered the sampling of filtered air for 5 min and the background signal, $E_{background,i}$, calculated by the following

$$E_{background,i} = E_i \pm 9\sigma_i$$

where E_i is the average signal in channel i, for a force-triggered sample, and σ_i is the SD of the force-triggered sample signal in channel i. $E_{background,i}$ was subtracted from each particle for each channel to yield the final fluorescence signal. Particles were classified into types based on their fluorescent signal in each channel using criteria defined in a previous study (*34*). In this work, we have focused upon a subset of fluorescent particles (FP3) characterized by very strong signal in the FL1 channel (FL1 > 1900). This class of particles has previously been linked to INP concentrations in ambient measurements (*34*, *35*).

Single-particle composition

Size-resolved, single-particle mass spectra were collected using an ATOFMS (*26*). Particles are introduced into the instrument through a nozzle and then subsequently collimated and focused by a series of skimmers. The particle beam is focused through the path of two continuous wave lasers (532 nm; Nd:YAG) 6 cm apart. As particles travel through the laser beam, they scatter light, which is reflected by ellipsoidal mirrors onto photomultiplier tubes (PMTs). The time between scattered light being detected at the two PMTs is used to calculate the particle velocity. Through external calibration with polystyrene latex spheres of known size and density, the particle velocity can be used to determine the particle vacuum aerodynamic diameter (D_{va}). The particle velocity also triggers a pulsed 266-nm laser (Nd:YAG; 1.0 to 1.3 mJ $pulse^{-1}$) to desorb and ionize particles into a dual-polarity time-of-flight mass spectrometer. Both positive and negative ions are generated by the laser desorption process. For each particle, the dual-polarity mass spectrum, D_{va}, and time stamp are recorded. These data were imported into MATLAB (The MathWorks Inc.) and analyzed using the software toolkit FATES (*70*). Particles were clustered on the basis of their mass spectral features via an adaptive neural network (*71*). Particle types were manually regrouped upon inspection of the clusters based on spectral similarities (*65*). In this work, we focus only upon those particles identified as dust or SSA.

Predicting INP concentrations using single-particle measurements

On the basis of previous work identifying INP sources at Bodega Bay (*20*), we assume that the INP concentrations at this site can be described by dust, SSA, and bioaerosol. While some recent studies have highlighted how using time-dependent IN parameterizations may be able to account for effects of factors such as uneven distribution of surface area among particles (*72*, *73*), we use a deterministic approach here.

The active site density (n_s), conceptualized as the density of ice-active sites within a given particle type population per unit surface area, can be used to predict INP concentrations by the following

$$N_{INP,x} = n_{s,x} A_x$$

where $n_{s,x}$ is the active site density for particle type x and A_x is the total particle surface area per unit volume.

We calculate A_x from combined measurements of the ATOFMS and APS. Single-particle mass spectrometry (SPMS) techniques such as the ATOFMS do not provide quantitative concentrations of different particle types, although SPMS measurements can be used in tandem with size distributions from co-located instruments to return quantitative concentrations of particle types (*29*, *74*). A_x can be described by

$$A_x = \sum_{i=1}^{51} D_{p,x,i}^2 \pi n_i f_{x,i}$$

where $D_{p,x,i}$ is the particle diameter of class x in size bin i, and $f_{x,i}$ is the size-resolved fraction of particle class x in that same size bin. For APS size bins larger than the upper limit of the ATOFMS, we follow the example of a previous study (*8*) and calculate $f_{x,i}$ using ATOFMS particles larger than 1 μm. $D_{p,x}$ can be calculated from

$$D_{p,x} = D_{a,x} \sqrt{\frac{\rho_0 \chi_x}{\rho_x}}$$

where $D_{a,x,}$ is the aerodynamic diameter of particle type x, ρ_0 is the unit density, χ_x is the dynamic shape factor of class x, and ρ_x is the density of class x. We assumed χ_{dust} to be 1.25, χ_{SSA} to be 1.25, ρ_{dust} to be 2.65 g cm^{-3}, and ρ_{SSA} to be 2.2 g cm^{-3}. $D_{a,x}$ was calculated from the ATOFMS-measured values of type-dependent vacuum

aerodynamic diameter $D_{va,x}$ by

$$D_{a,x} = D_{va,x}\sqrt{\frac{\chi_x}{\rho_x}}$$

We assumed that the dynamic shape factors for the continuum and free-molecular regimes are roughly equal. We note that this assumption does not always hold (*75*).

We use the n_s-based parameterizations from N12 (*27*) and M18 (*28*) to predict INP concentrations from dust and SSA, respectively. We did not observe enough bioaerosol with the ATOFMS to calculate a particle type–specific surface area. However, we do see a strong relationship between fluorescent particles measured by the WIBS and INP concentrations. The correlations between these measurements are particularly strong for the FP3 particle class (*34*) and INPs measured at warmer temperatures (Fig. 3). Thus, we devise a simple scalar-based parameterization of FP3 particles for bio-INPs, i.e.

$$N_{INP,Bio} = \gamma FP3$$

where γ is the scalar. As mentioned above, we assume that the INP population at Bodega Bay can be adequately described by assuming that the relevant sources of INPs are dust, SSA, and bioaerosol

$$N_{INP} = N_{INP,dust} + N_{INP,SSA} + N_{INP,Bio}$$

We can calculate $N_{INP,dust}$ and $N_{INP,SSA}$ by rewriting the above to

$$N_{INP,Bio} = N_{INP} - (N_{INP,dust} + N_{INP,SSA})$$

This can then be combined with the above to yield

$$FP3 = \frac{N_{INP} - (N_{INP,dust} + N_{INP,SSA})}{\gamma}$$

Calculated values for γ ranged from 0.00465 at −12°C to 0.3108 at −20°C (fig. S2). This methodology implicitly assumes that FP3 is an equally representative proxy for all bio-INPs. Future research should investigate this assumption in greater detail through further laboratory and field experiments.

Comparison with previous methods of quantifying bio-INPs

Previous studies of bio-INPs in the ambient atmosphere have relied on indirect methods, such as heat and peroxide treatments, to quantify their concentrations [e.g., (*17*)]. We performed heat treatments for a subset of our IS samples for comparison with our methodology. Figure S4 shows the results of six samples, separated into either high or low bioaerosol concentrations. Nearly all of the INPs at −12°C were inactivated by the heat treatment. The high bioaerosol samples had high bio-INP fractions across the entire temperature range. The low bioaerosol concentration samples had more INPs coming from nonbiological sources. While we are not able to provide a direct comparison between the two methodologies of speciating INPs due to the different sampling times and methodologies for the INP measurements, the results from the heat treatment experiments are broadly consistent with the results acquired using our scalar-based methodology.

Single-particle composition of ice crystal residuals

We used an SPMS to directly characterize ice crystal residuals [e.g., (*76*)]. These results have been described in detail elsewhere, so we provide a short description of the methods (*20*). We used a CFDC (*77*) to activate INPs into ice crystals, which were then separated from nonactivated particles via a pumped counterflow virtual impactor (PCVI; Brechtel Manufacturing Inc., model 8100). The CFDC was operated at approximately −31°C, with water supersaturation ranging between ~3 and ~7%. These ice crystals were melted and dried with a silica diffusion dryer, and the residual particle composition was measured by an ATOFMS. A 1.5-μm impactor was placed upstream of the CFDC to remove large particles, which might be mistakenly counted as INPs or transmitted through the PCVI counterflow. Residuals were sampled for a few hours each day from 12 to 19 February 2015 (total residual sampling time: 16 hours and 28 min). Control periods measuring ambient aerosol composition were selected on the basis of wind speed and wind direction (total ambient sampling time: 30 hours and 6 min).

Single-particle mass spectra and size data were imported into MATLAB and analyzed with the software toolkit FATES (*70*). Particles were clustered on the basis of their mass spectral features using an adaptive neural network and combined manually into particle types. In this work, we focus on particles classified as dust and SSA. Across all sampling days, dust was the most abundant type in the ice crystal residuals by number fraction (70.5%). Speciated INP concentrations were calculated for each CFDC sampling period by scaling the reported INP concentrations by the ice crystal residual fraction (calculated daily). We apply a correction factor of 3 to correct for incomplete activation of dust particles in the CFDC chamber (*78*). Speciated particle surface areas were calculated for CFDC measurements periods by mapping the single-particle composition measured by the ATOFMS during control periods onto the APS size distributions (see the previous section for more details on this procedure). To increase the number of INPs characterized, ambient particle concentrations were enhanced using an aerosol concentrator (model 4240, MSP Corporation).

Supplementary Materials

This PDF file includes:

Supplementary Text
Figs. S1 to S13
References

REFERENCES AND NOTES

1. P. J. DeMott, A. J. Prenni, X. Liu, S. M. Kreidenweis, M. D. Petters, C. H. Twohy, M. Richardson, T. Eidhammer, D. Rogers, Predicting global atmospheric ice nuclei distributions and their impacts on climate. *Proc. Natl. Acad. Sci. U.S.A.* **107**, 11217–11222 (2010).
2. Y.-S. Choi, R. S. Lindzen, C.-H. Ho, J. Kim, Space observations of cold-cloud phase change. *Proc. Natl. Acad. Sci. U.S.A.* **107**, 11211–11216 (2010).
3. J. Vergara-Temprado, A. K. Miltenberger, K. Furtado, D. P. Grosvenor, B. J. Shipway, A. A. Hill, J. M. Wilkinson, P. R. Field, B. J. Murray, K. S. Carslaw, Strong control of Southern Ocean cloud reflectivity by ice-nucleating particles. *Proc. Natl. Acad. Sci. U.S.A.* **115**, 2687–2692 (2018).
4. R. E. Hawker, A. K. Miltenberger, J. M. Wilkinson, A. A. Hill, B. J. Shipway, Z. Cui, R. J. Cotton, K. S. Carslaw, P. R. Field, B. J. Murray, The temperature dependence of ice-nucleating particle concentrations affects the radiative properties of tropical convective cloud systems. *Atmos. Chem. Phys.* **21**, 5439–5461 (2021).
5. J. Fan, L. R. Leung, D. Rosenfeld, P. J. Demott, Effects of cloud condensation nuclei and ice nucleating particles on precipitation processes and supercooled liquid in mixed-phase orographic clouds. *Atmos. Chem. Phys.* **17**, 1017–1035 (2017).
6. I. Tan, D. Barahona, Q. Coopman, Potential link between ice nucleation and climate model spread in arctic amplification. *Geophys. Res. Lett.* **49**, e2021GL097373 (2022).
7. L. B. Hande, C. Hoose, Partitioning the primary ice formation modes in large eddy simulations of mixed-phase clouds. *Atmos. Chem. Phys.* **17**, 14105–14118 (2017).

8. D. A. Knopf, K. R. Barry, T. A. Brubaker, L. G. Jahl, K. A. Jankowski, J. Li, Y. Lu, L. W. Monroe, K. A. Moore, F. A. Rivera-Adorno, K. A. Sauceda, Y. Shi, J. M. Tomlin, H. S. K. Vepuri, P. Wang, N. N. Lata, E. J. T. Levin, J. M. Creamean, T. C. J. Hill, S. China, P. A. Alpert, R. C. Moffet, N. Hiranuma, R. C. Sullivan, A. M. Fridlind, M. West, N. Riemer, A. Laskin, P. J. DeMott, X. Liu, Aerosol–ice formation closure: A southern great plains field campaign. *Bull. Am. Meteorol. Soc.* **102**, E1952–E1971 (2021).
9. S. M. Burrows, C. S. McCluskey, G. Cornwell, I. Steinke, K. Zhang, B. Zhao, M. Zawadowicz, A. Raman, G. Kulkarni, S. China, A. Zelenyuk, P. J. DeMott, Ice-nucleating particles that impact clouds and climate: Observational and modeling research needs. *Rev. Geophys.* **60**, e2021RG000745 (2022).
10. B. J. Murray, D. O'Sullivan, J. D. Atkinson, M. E. Webb, Ice nucleation by particles immersed in supercooled cloud droplets. *Chem. Soc. Rev.* **41**, 6519–6554 (2012).
11. Z. A. Kanji, L. A. Ladino, H. Wex, Y. Boose, M. Burkert-Kohn, D. J. Cziczo, M. Krämer, Overview of ice nucleating particles. *Meteorol. Monogr.* **58**, 1.1–1.33 (2017).
12. S. Huang, W. Hu, J. Chen, Z. Wu, D. Zhang, P. Fu, Overview of biological ice nucleating particles in the atmosphere. *Environ. Int.* **146**, 106197 (2021).
13. D. V. Spracklen, C. L. Heald, The contribution of fungal spores and bacteria to regional and global aerosol number and ice nucleation immersion freezing rates. *Atmos. Chem. Phys.* **14**, 9051–9059 (2014).
14. A. Korolev, T. Leisner, Review of experimental studies of secondary ice production. *Atmos. Chem. Phys.* **20**, 11767–11797 (2020).
15. A. Takeishi, T. Storelvmo, A study of enhanced heterogeneous ice nucleation in simulated deep convective clouds observed during DC3. *J. Geophys. Res. Atmos.* **123**, 13396–13420 (2018).
16. J. Wieder, N. Ihn, C. Mignani, M. Haarig, J. Bühl, P. Seifert, R. Engelmann, F. Ramelli, Z. A. Kanji, U. Lohmann, J. Henneberger, Retrieving ice-nucleating particle concentration and ice multiplication factors using active remote sensing validated by in situ observations. *Atmos. Chem. Phys.* **22**, 9767–9797 (2022).
17. T. C. J. Hill, P. J. DeMott, Y. Tobo, J. Fröhlich-Nowoisky, B. F. Moffett, G. D. Franc, S. M. Kreidenweis, Sources of organic ice nucleating particles in soils. *Atmos. Chem. Phys.* **16**, 7195–7211 (2016).
18. M. I. Daily, M. D. Tarn, T. F. Whale, B. J. Murray, An evaluation of the heat test for the ice-nucleating ability of minerals and biological material. *Atmos. Meas. Tech.* **15**, 2635–2665 (2022).
19. R. H. Mason, M. Si, J. Li, C. Chou, R. Dickie, D. Toom-Sauntry, C. Pöhlker, J. D. Yakobi-Hancock, L. A. Ladino, K. Jones, W. R. Leaitch, C. L. Schiller, J. P. D. Abbatt, J. A. Huffman, A. K. Bertram, Ice nucleating particles at a coastal marine boundary layer site: Correlations with aerosol type and meteorological conditions. *Atmos. Chem. Phys.* **15**, 12547–12566 (2015).
20. G. C. Cornwell, C. S. McCluskey, E. J. T. Levin, K. J. Suski, P. J. DeMott, S. M. Kreidenweis, K. A. Prather, Direct online mass spectrometry measurements of ice nucleating particles at a california coastal site. *J. Geophys. Res. Atmos.* **124**, 12157–12172 (2019).
21. Z. A. Kanji, R. C. Sullivan, M. Niemand, P. J. DeMott, A. J. Prenni, C. Chou, H. Saathoff, O. Möhler, Heterogeneous ice nucleation properties of natural desert dust particles coated with a surrogate of secondary organic aerosol. *Atmos. Chem. Phys.* **19**, 5091–5110 (2019).
22. G. P. Schill, P. J. DeMott, E. W. Emerson, A. M. C. Rauker, J. K. Kodros, K. J. Suski, T. C. Hill, E. J. Levin, J. R. Pierce, D. K. Farmer, The contribution of black carbon to global ice nucleating particle concentrations relevant to mixed-phase clouds. *Proc. Natl. Acad. Sci. U.S.A.* **117**, 22705–22711 (2020).
23. S. Kasparoglu, R. Perkins, P. J. Ziemann, P. J. DeMott, S. M. Kreidenweis, Z. Finewax, B. L. Deming, M. P. DeVault, M. D. Petters, Experimental determination of the relationship between organic aerosol viscosity and ice nucleation at upper free tropospheric conditions. *J. Geophys. Res. Atmos.* **127**, e2021JD036296 (2022).
24. C. Wu, Z. Lin, X. Liu, The global dust cycle and uncertainty in CMIP5 (coupled model intercomparison project phase 5) models. *Atmos. Chem. Phys.* **20**, 10401–10425 (2020).
25. B. Testa, T. C. J. Hill, N. A. Marsden, K. R. Barry, C. C. Hume, Q. Bian, J. Uetake, H. Hare, R. J. Perkins, O. Möhler, S. M. Kreidenweis, P. J. DeMott, Ice nucleating particle connections to regional argentinian land surface emissions and weather during the cloud, aerosol, and complex terrain interactions experiment. *J. Geophys. Res. Atmos.* **126**, e2021JD035186 (2022).
26. E. Gard, J. E. Mayer, B. D. Morrical, T. Dienes, D. P. Fergenson, K. A. Prather, Real-time analysis of individual atmospheric aerosol particles: Design and performance of a portable ATOFMS. *Anal. Chem.* **69**, 4083–4091 (1997).
27. M. Niemand, O. Möhler, B. Vogel, H. Vogel, C. Hoose, P. Connolly, H. Klein, H. Bingemer, P. DeMott, J. Skrotzki, T. Leisner, A particle-surface-area-based parameterization of immersion freezing on desert dust particles. *J. Atmos. Sci.* **69**, 3077–3092 (2012).
28. C. S. McCluskey, J. Ovadnevaite, M. Rinaldi, J. Atkinson, F. Belosi, D. Ceburnis, S. Marullo, T. C. J. Hill, U. Lohmann, Z. A. Kanji, C. O'Dowd, S. M. Kreidenweis, P. J. DeMott, Marine and terrestrial organic ice-nucleating particles in pristine marine to continentally influenced northeast atlantic air masses. *J. Geophys. Res. Atmos.* **123**, 6196–6212 (2018).
29. K. D. Froyd, D. M. Murphy, C. A. Brock, P. Campuzano-Jost, J. E. Dibb, J.-L. Jimenez, A. Kupc, A. M. Middlebrook, G. P. Schill, K. L. Thornhill, C. J. Williamson, J. C. Wilson, L. D. Ziemba, A new method to quantify mineral dust and other aerosol species from aircraft platforms using single-particle mass spectrometry. *Atmos. Meas. Tech.* **12**, 6209–6239 (2019).
30. G. C. Cornwell, C. S. McCluskey, P. J. DeMott, K. A. Prather, S. M. Burrows, Development of heterogeneous ice nucleation rate coefficient parameterizations from ambient measurements. *Geophys. Res. Lett.* **48**, e2021GL095359 (2021).
31. J. Vergara-Temprado, B. J. Murray, T. W. Wilson, D. O'Sullivan, J. Browse, K. J. Pringle, K. Ardon-Dryer, A. K. Bertram, S. M. Burrows, D. Ceburnis, P. J. Demott, R. H. Mason, C. D. O'Dowd, M. Rinaldi, K. S. Carslaw, Contribution of feldspar and marine organic aerosols to global ice nucleating particle concentrations. *Atmos. Chem. Phys.* **17**, 3637–3658 (2017).
32. S. Yadav, R. E. Venezia, R. W. Paerl, M. D. Petters, Characterization of ice-nucleating particles over Northern India. *J. Geophys. Res. Atmos.* **124**, 10467–10482 (2019).
33. G. C. Cornwell, C. M. Sultana, M. D. Petters, H. Al-Mashat, N. E. Rothfuss, O. Möhler, P. J. DeMott, A. C. Martin, K. A. Prather, Discrimination between individual dust and bioparticles using aerosol time-of-flight mass spectrometry. *Aerosol Sci. Tech.* **56**, 592–608 (2022).
34. T. P. Wright, J. D. Hader, G. R. McMeeking, M. D. Petters, High relative humidity as a trigger for widespread release of ice nuclei. *Aerosol. Sci. Tech.* **48**, i–v (2014).
35. K. J. Suski, T. C. J. Hill, E. J. T. Levin, A. Miller, P. J. DeMott, S. M. Kreidenweis, Agricultural harvesting emissions of ice-nucleating particles. *Atmos. Chem. Phys.* **18**, 13755–13771 (2018).
36. X. Gong, M. Radenz, H. Wex, P. Seifert, F. Ataei, S. Henning, H. Baars, B. Barja, A. Ansmann, F. Stratmann, Significant continental source of ice-nucleating particles at the tip of Chile's southernmost Patagonia region. *Atmos. Chem. Phys.* **22**, 10505–10525 (2022).
37. J. A. Huffman, A. J. Prenni, P. J. Demott, C. Pöhlker, R. H. Mason, N. H. Robinson, J. Fröhlich-Nowoisky, Y. Tobo, V. R. Després, E. Garcia, D. J. Gochis, E. Harris, I. Müller-Germann, C. Ruzene, B. Schmer, B. Sinha, D. A. Day, M. O. Andreae, J. L. Jimenez, M. Gallagher, S. M. Kreidenweis, A. K. Bertram, U. Pöschl, High concentrations of biological aerosol particles and ice nuclei during and after rain. *Atmos. Chem. Phys.* **13**, 6151–6164 (2013).
38. K. Hara, T. Maki, F. Kobayashi, M. Kakikawa, M. Wada, A. Matsuki, Variations of ice nuclei concentration induced by rain and snowfall within a local forested site in Japan. *Atmos. Environ.* **127**, 1–5 (2016).
39. C. M. Rathnayake, N. Metwali, T. Jayarathne, J. Kettler, Y. Huang, P. S. Thorne, P. T. O'Shaughnessy, E. A. Stone, Influence of rain on the abundance of bioaerosols in fine and coarse particles. *Atmos. Chem. Phys.* **17**, 2459–2475 (2017).
40. I. Pisso, E. Sollum, H. Grythe, N. I. Kristiansen, M. Cassiani, S. Eckhardt, D. Arnold, D. Morton, R. L. Thompson, C. D. Groot Zwaaftink, N. Evangeliou, H. Sodemann, L. Haimberger, S. Henne, D. Brunner, J. F. Burkhart, A. Fouilloux, J. Brioude, A. Philipp, P. Seibert, A. Stohl, The Lagrangian particle dispersion model FLEXPART version 10.4. *Geosci. Model Dev.* **12**, 4955–4997 (2019).
41. P. Seibert, A. Frank, Source-receptor matrix calculation with a Lagrangian particle dispersion model in backward mode. *Atmos. Chem. Phys.* **4**, 51–63 (2004).
42. S. M. Burrows, T. Butler, P. Jöckel, H. Tost, A. Kerkweg, U. Pöschl, M. G. Lawrence, Bacteria in the global atmosphere–Part 2: Modeling of emissions and transport between different ecosystems. *Atmos. Chem. Phys.* **9**, 9281–9297 (2009).
43. R. H. H. Janssen, C. L. Heald, A. L. Steiner, A. E. Perring, J. A. Huffman, E. S. Robinson, C. H. Twohy, L. D. Ziemba, Drivers of the fungal spore bioaerosol budget: Observational analysis and global modeling. *Atmos. Chem. Phys.* **21**, 4381–4401 (2021).
44. C. Hoose, O. Möhler, Heterogeneous ice nucleation on atmospheric aerosols: A review of results from laboratory experiments. *Atmos. Chem. Phys.* **12**, 9817–9854 (2012).
45. S. Patade, V. Phillips, S. M. Burrows, C. Morris, D. Knopf, P. Amato, F. Goncalves, H. Bingemer, J. Schrod, P. DeMott, C. Alwmark, C. Pöhlker, Empirical formulation for multiple groups of primary biological ice nuclei from field observations over Amazonia. *J. Atmos. Sci.* **78**, 2195–2220 (2021).
46. S. Augustin-Bauditz, H. Wex, S. Kanter, M. Ebert, D. Niedermeier, F. Stolz, A. Prager, F. Stratmann, The immersion mode ice nucleation behavior of mineral dusts: A comparison of different pure and surface modified dusts. *Geophys. Res. Lett.* **41**, 7375–7382 (2014).
47. L. G. Jahl, T. A. Brubaker, M. J. Polen, L. G. Jahn, K. P. Cain, B. B. Bowers, W. D. Fahy, S. Graves, R. C. Sullivan, Atmospheric aging enhances the ice nucleation ability of biomass-burning aerosol. *Sci. Adv.* **7**, eabd3440 (2021).
48. M. Joly, E. Attard, M. Sancelme, L. Deguillaume, C. Guilbaud, C. E. Morris, P. Amato, A.-M. Delort, Ice nucleation activity of bacteria isolated from cloud water. *Atmos. Environ.* **70**, 392–400 (2013).

49. B. G. Pummer, H. Bauer, J. Bernardi, S. Bleicher, H. Grothe, Suspendable macromolecules are responsible for ice nucleation activity of birch and conifer pollen. *Atmos. Chem. Phys.* **12**, 2541–2550 (2012).
50. K. Dietzel, D. Valle, N. Fierer, J. M. U'ren, A. Barberán, Geographical distribution of fungal plant pathogens in dust across the United States. *Front. Ecol. Evol.* **7**, 1–8 (2019).
51. A. Barberán, J. Ladau, J. W. Leff, K. S. Pollard, H. L. Menninger, R. R. Dunn, N. Fierer, Continental-scale distributions of dust-associated bacteria and fungi. *Proc. Natl. Acad. Sci. U.S.A.* **112**, 5756–5761 (2015).
52. E. Gute, R. O. David, Z. A. Kanji, J. P. D. Abbatt, Ice nucleation ability of tree pollen altered by atmospheric processing. *ACS Earth Space Chem.* **4**, 2312–2319 (2020).
53. P. T. Mckenney, A. Driks, P. Eichenberger, The *Bacillus subtilis* endospore: Assembly and functions of the multilayered coat. *Nat. Rev. Microbiol.* **11**, 33–44 (2013).
54. P. Roy, L. E. Mael, T. C. J. Hill, L. Mehndiratta, G. Peiker, M. L. House, P. J. DeMott, V. H. Grassian, C. S. Dutcher, Ice nucleating activity and residual particle morphology of bulk seawater and sea surface microlayer. *ACS Earth Space Chem.* **5**, 1916–1928 (2021).
55. C. H. Twohy, G. R. McMeeking, P. J. DeMott, C. S. McCluskey, T. C. J. Hill, S. M. Burrows, G. R. Kulkarni, M. Tanarhte, D. N. Kafle, D. W. Toohey, Abundance of fluorescent biological aerosol particles at temperatures conducive to the formation of mixed-phase and cirrus clouds. *Atmos. Chem. Phys.* **16**, 8205–8225 (2016).
56. A. E. Perring, J. P. Schwarz, D. Baumgardner, M. T. Hernandez, D. V. Spracklen, C. L. Heald, R. S. Gao, G. Kok, G. R. McMeeking, J. B. McQuaid, D. W. Fahey, Airborne observations of regional variation in fluorescent aerosol across the United States. *J. Geophys. Res. Atmos.* **120**, 1153–1170 (2015).
57. K. C. Failor, D. G. Schmale, B. A. Vinatzer, C. L. Monteil, Ice nucleation active bacteria in precipitation are genetically diverse and nucleate ice by employing different mechanisms. *ISME J.* **11**, 2740–2753 (2017).
58. S. Yadav, N. P. Curtis, R. E. Venezia, A. Tandon, R. W. Paerl, M. D. Petters, Bioaerosol diversity and ice nucleating particles in the North-Western Himalayan region. *J. Geophys. Res. Atmospheres* **127**, e2021JD036299 (2022).
59. B. H. Matthews, A. N. Alsante, S. D. Brooks, Pollen emissions of subpollen particles and ice nucleating particles. *ACS Earth Space Chem.* **7**, 1207–1218 (2023).
60. D. O'Sullivan, B. J. Murray, J. F. Ross, T. F. Whale, H. C. Price, J. D. Atkinson, N. S. Umo, M. E. Webb, The relevance of nanoscale biological fragments for ice nucleation in clouds. *Sci. Rep.* **5**, 1–7 (2015).
61. N. Hiranuma, O. Möhler, K. Yamashita, T. Tajiri, A. Saito, A. Kiselev, N. Hoffmann, C. Hoose, E. Jantsch, T. Koop, M. Murakami, Ice nucleation by cellulose and its potential contribution to ice formation in clouds. *Nat. Geosci.* **8**, 273–277 (2015).
62. C. S. McCluskey, T. C. J. Hill, C. M. Sultana, O. Laskina, J. Trueblood, M. V. Santander, C. M. Beall, J. M. Michaud, S. M. Kreidenweis, K. A. Prather, V. Grassian, P. J. DeMott, A mesocosm double feature: Insights into the chemical makeup of marine ice nucleating particles. *J. Atmos. Sci.* **75**, 2405–2423 (2018).
63. F. Conen, A. Einbock, C. Mignani, C. Hüglin, Measurement report: Ice-nucleating particles active ≥ −15 °C in free tropospheric air over western Europe. *Atmos. Chem. Phys.* **22**, 3433–3444 (2022).
64. J. M. Creamean, K. Barry, T. C. J. Hill, C. Hume, P. J. DeMott, M. D. Shupe, S. Dahlke, S. Willmes, J. Schmale, I. Beck, C. J. M. Hoppe, A. Fong, E. Chamberlain, J. Bowman, R. Scharien, O. Persson, Annual cycle observations of aerosols capable of ice formation in central Arctic clouds. *Nat. Commun.* **13**, 3537 (2022).
65. A. C. Martin, G. C. Cornwell, S. A. Atwood, K. A. Moore, N. E. Rothfuss, H. Taylor, P. J. DeMott, S. M. Kreidenweis, M. D. Petters, K. A. Prather, Transport of pollution to a remote coastal site during gap flow from California's interior: Impacts on aerosol composition, clouds, and radiative balance. *Atmos. Chem. Phys.* **17**, 1491–1509 (2017).
66. G. Vali, Quantitative evaluation of experimental results an the heterogeneous freezing nucleation of supercooled liquids. *J. Atmos. Sci.* **28**, 402–409 (1971).
67. A. Agresti, B. A. Coull, Approximate is better than "exact" for interval estimation of binomial proportions. *Am. Stat.* **52**, 119–126 (1998).
68. A. M. Gabey, W. R. Stanley, M. W. Gallagher, P. H. Kaye, The fluorescence properties of aerosol larger than 0.8 μ in urban and tropical rainforest locations. *Atmos. Chem. Phys.* **11**, 5491–5504 (2011).
69. N. J. Savage, C. E. Krentz, T. Könemann, T. T. Han, G. Mainelis, C. Pöhlker, J. Alex Huffman, Systematic characterization and fluorescence threshold strategies for the wideband integrated bioaerosol sensor (WIBS) using size-resolved biological and interfering particles. *Meas. Tech.* **10**, 4279–4302 (2017).
70. C. M. Sultana, G. C. Cornwell, P. Rodriguez, K. A. Prather, FATES: A flexible analysis toolkit for the exploration of single-particle mass spectrometer data. *Atmos. Meas. Tech.* **10**, 1323–1334 (2017).
71. X. H. Song, P. K. Hopke, D. P. Fergenson, K. a. Prather, Classification of single particles analyzed by ATOFMS using an artificial neural network, ART-2A. *Anal. Chem.* **71**, 860–865 (1999).
72. P. A. Alpert, D. A. Knopf, Analysis of isothermal and cooling-rate-dependent immersion freezing by a unifying stochastic ice nucleation model. *Atmos. Chem. Phys.* **16**, 2083–2107 (2016).
73. D. A. Knopf, P. A. Alpert, A. Zipori, N. Reicher, Y. Rudich, Stochastic nucleation processes and substrate abundance explain time-dependent freezing in supercooled droplets. *Npj Clim. Atmos. Sci.* **3**, 1–9 (2020).
74. X. Qin, P. V. Bhave, K. A. Prather, Comparison of two methods for obtaining quantitative mass concentrations from aerosol time-of-flight mass spectrometry measurements. *Anal. Chem.* **78**, 6169–6178 (2006).
75. J. M. Alexander, D. M. Bell, D. Imre, P. D. Kleiber, V. H. Grassian, A. Zelenyuk, D. M. Bell, D. Imre, P. D. Kleiber, V. H. Grassian, Measurement of size-dependent dynamic shape factors of quartz particles in two flow regimes. *Aerosol. Sci. Tech.* **50**, 870–879 (2016).
76. D. J. Cziczo, P. J. DeMott, C. Brock, P. K. Hudson, B. Jesse, S. M. Kreidenweis, A. J. Prenni, J. Schreiner, D. S. Thomson, D. M. Murphy, A method for single particle mass spectrometry of ice nuclei. *Aerosol. Sci. Tech.* **37**, 460–470 (2003).
77. T. Eidhammer, P. J. DeMott, S. M. Kreidenweis, A comparison of heterogeneous ice nucleation parameterizations using a parcel model framework. *J. Geophys. Res.* **114**, D06202 (2009).
78. P. J. DeMott, A. J. Prenni, G. R. McMeeking, R. C. Sullivan, M. D. Petters, Y. Tobo, M. Niemand, O. Möhler, J. R. Snider, Z. Wang, S. M. Kreidenweis, Integrating laboratory and field data to quantify the immersion freezing ice nucleation activity of mineral dust particles. *Atmos. Chem. Phys.* **15**, 393–409 (2015).
79. J. C. Golaz, P. M. Caldwell, L. P. Van Roekel, M. R. Petersen, Q. Tang, J. D. Wolfe, G. Abeshu, V. Anantharaj, X. S. Asay-Davis, D. C. Bader, S. A. Baldwin, G. Bisht, P. A. Bogenschutz, M. Branstetter, M. A. Brunke, S. R. Brus, S. M. Burrows, P. J. Cameron-Smith, A. S. Donahue, M. Deakin, R. C. Easter, K. J. Evans, Y. Feng, M. Flanner, J. G. Foucar, J. G. Fyke, B. M. Griffin, C. Hannay, B. E. Harrop, M. J. Hoffman, E. C. Hunke, R. L. Jacob, D. W. Jacobsen, N. Jeffery, P. W. Jones, N. D. Keen, S. A. Klein, V. E. Larson, L. R. Leung, H. Y. Li, W. Lin, W. H. Lipscomb, P. L. Ma, S. Mahajan, M. E. Maltrud, A. Mametjanov, J. L. McClean, R. B. McCoy, R. B. Neale, S. F. Price, Y. Qian, P. J. Rasch, J. E. J. R. Eyre, W. J. Riley, T. D. Ringler, A. F. Roberts, E. L. Roesler, A. G. Salinger, Z. Shaheen, X. Shi, B. Singh, J. Tang, M. A. Taylor, P. E. Thornton, A. K. Turner, M. Veneziani, H. Wan, H. Wang, S. Wang, D. N. Williams, P. J. Wolfram, P. H. Worley, S. Xie, Y. Yang, J. H. Yoon, M. D. Zelinka, C. S. Zender, X. Zeng, C. Zhang, K. Zhang, Y. Zhang, X. Zheng, T. Zhou, Q. Zhu, The DOE E3SM coupled model version 1: Overview and evaluation at standard resolution. *J. Adv. Model. Earth Syst.* **11**, 2089–2129 (2019).
80. P. J. Rasch, S. Xie, P. L. Ma, W. Lin, H. Wang, Q. Tang, S. M. Burrows, P. Caldwell, K. Zhang, R. C. Easter, P. Cameron-Smith, B. Singh, H. Wan, J. C. Golaz, B. E. Harrop, E. Roesler, J. Bacmeister, V. E. Larson, K. J. Evans, Y. Qian, M. Taylor, L. R. Leung, Y. Zhang, L. Brent, M. Branstetter, C. Hannay, S. Mahajan, A. Mametjanov, R. Neale, J. H. Richter, J. H. Yoon, C. S. Zender, D. Bader, M. Flanner, J. G. Foucar, R. Jacob, N. Keen, S. A. Klein, X. Liu, A. G. Salinger, M. Shrivastava, Y. Yang, An overview of the atmospheric component of the energy exascale earth system model. *J. Adv. Model. Earth Syst.* **11**, 2377–2411 (2019).
81. P. J. Lawrence, T. N. Chase, Representing a new MODIS consistent land surface in the Community Land Model (CLM 3.0). *J. Geophys. Res.* **112**, G01023 (2007).
82. R. Gelaro, W. McCarty, M. J. Suárez, R. Todling, A. Molod, L. Takacs, C. A. Randles, A. Darmenov, M. G. Bosilovich, R. Reichle, K. Wargan, L. Coy, R. Cullather, C. Draper, S. Akella, V. Buchard, A. Conaty, A. M. da Silva, W. Gu, G. K. Kim, R. Koster, R. Lucchesi, D. Merkova, J. E. Nielsen, G. Partyka, S. Pawson, W. Putman, M. Rienecker, S. D. Schubert, M. Sienkiewicz, B. Zhao, The modern-era retrospective analysis for research and applications, version 2 (MERRA-2). *J. Climate* **30**, 5419–5454 (2017).
83. P. L. Ma, P. J. Rasch, M. Wang, H. Wang, S. J. Ghan, R. C. Easter, W. I. Gustafson, X. Liu, Y. Zhang, H. Y. Ma, How does increasing horizontal resolution in a global climate model improve the simulation of aerosol-cloud interactions? *Geophys. Res. Lett.* **42**, 5058–5065 (2015).
84. J. Sun, K. Zhang, H. Wan, P. Ma, Q. Tang, S. Zhang, Impact of nudging strategy on the climate representativeness and hindcast skill of constrained EAMv1 simulations. *J. Adv. Model. Earth Syst.* **11**, 3911–3933 (2019).
85. X. Liu, P. L. Ma, H. Wang, S. Tilmes, B. Singh, R. C. Easter, S. J. Ghan, P. J. Rasch, Description and evaluation of a new four-mode version of the Modal Aerosol Module (MAM4) within version 5.3 of the community atmosphere model. *Geosci. Model Dev.* **9**, 505–522 (2016).
86. H. Wang, R. C. Easter, R. Zhang, P. Ma, B. Singh, K. Zhang, D. Ganguly, P. J. Rasch, S. M. Burrows, S. J. Ghan, S. Lou, Y. Qian, Y. Yang, Y. Feng, M. Flanner, L. R. Leung, X. Liu, M. Shrivastava, J. Sun, Q. Tang, S. Xie, J. Yoon, Aerosols in the E3SM version 1: New developments and their impacts on radiative forcing. *J. Adv. Model. Earth Syst.* **12**, e2019MS001851 (2020).
87. C. S. Zender, H. Bian, B. Newman, Mineral Dust Entrainment and Deposition (DEAD) model: Description and 1990s dust climatology. *J. Geophys. Res. Atmospheres* **108**, 4416 (2003).

88. E. M. Mårtensson, E. D. Nilsson, G. de Leeuw, L. H. Cohen, H. C. Hansson, Laboratory simulations and parameterization of the primary marine aerosol production. *J. Geophys. Res. Atmos.* **108**, 1–12 (2003).
89. E. C. Monahan, D. E. Spiel, K. L. Davidson, A model of marine aerosol generation via whitecaps and wave disruption, in *Oceanic Whitecaps*, E. C. Monahan, G. M. Niocaill, Eds. (Springer Netherlands, 1986), vol. 2 of Oceanographic Sciences Library, pp. 167–174.
90. S. M. Burrows, O. Ogunro, A. A. Frossard, L. M. Russell, P. J. Rasch, S. M. Elliott, A physically based framework for modeling the organic fractionation of sea spray aerosol from bubble film Langmuir equilibria. *Atmos. Chem. Phys.* **14**, 13601–13629 (2014).
91. J. Brioude, D. Arnold, A. Stohl, M. Cassiani, D. Morton, P. Seibert, W. Angevine, S. Evan, A. Dingwell, J. D. Fast, R. C. Easter, I. Pisso, J. Burkhart, G. Wotawa, The Lagrangian particle dispersion model FLEXPART-WRF version 3.1. *Geosci. Model Dev.* **6**, 1889–1904 (2013).
92. W. C. Skamarock, J. B. Klemp, J. Dudhi, D. O. Gill, D. M. Barker, M. G. Duda, X.-Y. Huang, W. Wang, J. G. Powers, "A description of the advanced research WRF version 3" (NCAR Technical Note, 2008), p. 113.
93. G. Thompson, P. R. Field, R. M. Rasmussen, W. D. Hall, Explicit forecasts of winter precipitation using an improved bulk microphysics scheme. Part II: Implementation of a new snow parameterization. *Mon. Weather Rev.* **136**, 5095–5115 (2008).
94. M. Nakanishi, H. Niino, Development of an improved turbulence closure model for the atmospheric boundary layer. *J. Meteorol. Soc. Jpn. Ser.* **87**, 895–912 (2009).
95. Z. Janjić, "Nonsingular implementation of the Mellor-Yamada level 2.5 scheme in the NCEP Meso model" (Office Note, National Centers for Environmental Prediction, 2001).
96. F. Chen, J. Dudhia, Coupling an advanced land surface–hydrology model with the Penn State–NCAR MM5 modeling system. Part I: Model implementation and sensitivity. *Mon. Weather Rev.* **129**, 569–585 (2001).
97. M. J. Iacono, J. S. Delamere, E. J. Mlawer, M. W. Shephard, S. A. Clough, W. D. Collins, Radiative forcing by long-lived greenhouse gases: Calculations with the AER radiative transfer models. *J. Geophys. Res. Atmos.* **113**, 2–9 (2008).
98. H. Shao, J. Derber, X.-Y. Huang, M. Hu, K. Newman, D. Stark, M. Lueken, C. Zhou, L. Nance, Y.-H. Kuo, B. Brown, Bridging research to operations transitions: Status and plans of community GSI. *Bull. Am. Meteorol. Soc.* **97**, 1427–1440 (2016).
99. S. L. Tai, Z. Feng, P. L. Ma, C. Schumacher, J. D. Fast, Representations of precipitation diurnal cycle in the amazon as simulated by observationally constrained cloud-system resolving and global climate models. *J. Adv. Model. Earth Syst.* **13**, 1–25 (2021).
100. R. Myneni, Y. Knyazikhin, T. Park, MCD15A3H MODIS/Terra+Aqua Leaf Area Index/FPAR 4-day L4 Global 500m SIN Grid V006 [Data set]. NASA EOSDIS Land Processes DAAC. (2015); doi:10.5067/MO1DIS/MCD15A3H.006.
101. D. W. Griffin, C. Gonzalez, N. Teigell, T. Petrosky, D. E. Northup, M. Lyles, Observations on the use of membrane filtration and liquid impingement to collect airborne microorganisms in various atmospheric environments. *Aerobiologia* **27**, 25–35 (2011).
102. Z. Wang, T. Reponen, S. A. Grinshpun, R. L. Górny, K. Willeke, Effect of sampling time and air humidity on the bioefficiency of filter samplers for bioaerosol collection. *J. Aerosol Sci.* **32**, 661–674 (2001).
103. P. J. DeMott, T. C. J. Hill, M. D. Petters, A. K. Bertram, Y. Tobo, R. H. Mason, K. J. Suski, C. S. McCluskey, E. J. T. Levin, G. P. Schill, Y. Boose, A. M. Rauker, A. J. Miller, J. Zaragoza, K. Rocci, N. E. Rothfuss, H. P. Taylor, J. D. Hader, C. Chou, J. A. Huffman, U. Pöschl, A. J. Prenni, S. M. Kreidenweis, Comparative measurements of ambient atmospheric concentrations of ice nucleating particles using multiple immersion freezing methods and a continuous flow diffusion chamber. *Atmos. Chem. Phys.* **17**, 11227–11245 (2017).
104. P. J. DeMott, O. Möhler, D. J. Cziczo, N. Hiranuma, M. D. Petters, S. S. Petters, F. Belosi, H. G. Bingemer, S. D. Brooks, C. Budke, M. Burkert-Kohn, K. N. Collier, A. Danielczok, O. Eppers, L. Felgitsch, S. Garimella, H. Grothe, P. Herenz, T. C. J. Hill, K. Höhler, Z. A. Kanji, A. Kiselev, T. Koop, T. B. Kristensen, K. Krüger, G. Kulkarni, E. J. T. Levin, B. J. Murray, A. Nicosia, D. O'Sullivan, A. Peckhaus, M. J. Polen, H. C. Price, N. Reicher, D. A. Rothenberg, Y. Rudich, G. Santachiara, T. Schiebel, J. Schrod, T. M. Seifried, F. Stratmann, R. C. Sullivan, K. J. Suski, M. Szakáll, H. P. Taylor, R. Ullrich, J. Vergara-Temprado, R. Wagner, T. F. Whale, D. Weber, A. Welti, T. W. Wilson, M. J. Wolf, J. Zenker, The Fifth International Workshop on Ice Nucleation phase 2 (FIN-02): Laboratory intercomparison of ice nucleation measurements. *Atmos. Meas. Tech.* **11**, 6231–6257 (2018).
105. N. Hiranuma, S. Augustin-Bauditz, H. Bingemer, C. Budke, J. Curtius, A. Danielczok, K. Diehl, K. Dreischmeier, M. Ebert, F. Frank, N. Hoffmann, K. Kandler, A. Kiselev, T. Koop, T. Leisner, O. Möhler, B. Nillius, A. Peckhaus, D. Rose, S. Weinbruch, H. Wex, Y. Boose, P. J. Demott, J. D. Hader, T. C. J. Hill, Z. A. Kanji, G. Kulkarni, E. J. T. Levin, C. S. McCluskey, M. Murakami, B. J. Murray, D. Niedermeier, M. D. Petters, D. O'Sullivan, A. Saito, G. P. Schill, T. Tajiri, M. A. Tolbert, A. Welti, T. F. Whale, T. P. Wright, K. Yamashita, A comprehensive laboratory study on the immersion freezing behavior of illite NX particles: A comparison of 17 ice nucleation measurement techniques. *Atmos. Chem. Phys.* **15**, 2489–2518 (2015).
106. V. Huijnen, H. Eskes, Skill scores and evaluation methodology for the MACC II project. *MACC-II Deliv. D85* **2**, (2012).

Acknowledgments: We thank the UC Davis Bodega Marine Laboratory for the use of laboratory and office space and shipping and physical plant support while collecting data, as well as the California Air Resources Board for the trailer used for sampling. We thank H. Taylor, K. Hoffman, M. Hester, M. Scott, H. Tekleab, M. Wu, and S. Goodnight for their assistance in performing the cold-stage experiments and H. Taylor for his help during sample collection. We also thank A. Raman for assistance in setting up the E3SM simulations and C. Johson for assistance with figure visualization. **Funding:** This work was supported by the Department of Energy, Office of Science, Office of Biological Research Program (to G.C.C., S.-L.T., and S.M.B.) and the National Science Foundation (award numbers 1451347, 1450760, and 1450690 to G.C.C., C.S.M., E.T.L., T.C.J.H., N.E.R., M.D.P., P.J.D., S.K., and K.A.P.). **Author contributions:** Conceptualization: P.J.D., M.D.P., S.K., K.A.P., and S.M.B. Data curation: G.C.C. Formal analysis: G.C.C. Investigation: G.C.C., C.S.M., T.C.J.H., E.T.L., N.E.R., and S.-L.T. Visualization: G.C.C. Funding acquisition: P.J.D., M.D.P., S.K., K.A.P., and S.M.B. Project administration: P.J.D., M.D.P., S.K., K.A.P., and S.M.B. Supervision: P.J.D., M.D.P., S.K., K.A.P., and S.M.B. Writing—original draft: G.C.C. and S.M.B. Writing—review and editing: G.C.C., S.M.B., P.J.D., M.D.P., S.K., K.A.P., N.E.R., T.C.J.H., and E.T.L. **Competing interests:** The authors declare that they have no competing interests. **Data and materials availability:** All data needed to evaluate the conclusions in the paper are present in the paper and/or the Supplementary Materials. All data used in this study will be made publicly available upon publication of this manuscript (https://doi.org/10.25584/1890223).

Submitted 19 December 2022
Accepted 16 August 2023
Published 15 September 2023
10.1126/sciadv.adg3715